

Neutron scattering studies on spin fluctuations in Sr₂RuO₄

K. Jenni,^{1,*} S. Kunkemöller,¹ P. Steffens,² Y. Sidis,³ R. Bewley,⁴ Z. Q. Mao,^{5,6,7} Y. Maeno,⁵ and M. Braden^{1,†}

¹*II. Physikalisches Institut, Universität zu Köln, Zùlpicher Strasse 77, D-50937 Köln, Germany*

²*Institut Laue Langevin, 71 avenue des Martyrs, 38000 Grenoble, France*

³*Laboratoire Léon Brillouin, CEA/CNRS, F-91191 Gif-sur-Yvette Cedex, France*

⁴*ISIS Neutron and Muon Source, Rutherford Appleton Laboratory, Harwell Oxford, Didcot OX11 0QX, United Kingdom*

⁵*Department of Physics, Graduate School of Science, Kyoto University, Kyoto 606-8502, Japan*

⁶*Department of Physics, Tulane University, New Orleans, Louisiana 70118, USA*

⁷*Department of Physics, Pennsylvania State University, University Park, Pennsylvania 16802, USA*



(Received 17 December 2020; revised 12 February 2021; accepted 9 March 2021; published 18 March 2021)

The magnetic excitations in Sr₂RuO₄ are studied by polarized and unpolarized neutron scattering experiments as a function of temperature. At the scattering vector of the Fermi-surface nesting with a half-integer out-of-plane component, there is no evidence for the appearance of a resonance excitation in the superconducting phase. The body of existing data indicates weakening of the scattered intensity in the nesting spectrum to occur at very low energies. The nesting signal persists up to 290 K but is strongly reduced. In contrast, a quasiferromagnetic contribution maintains its strength and still exhibits a finite width in momentum space.

DOI: [10.1103/PhysRevB.103.104511](https://doi.org/10.1103/PhysRevB.103.104511)

I. INTRODUCTION

A quarter century after the discovery of superconductivity in Sr₂RuO₄ [1], its character and its pairing mechanism remain mysterious. Inspired by the ferromagnetic order appearing in the metallic sister compound SrRuO₃ [2], it was initially proposed that ferromagnetic fluctuations drive the superconductivity in Sr₂RuO₄ rendering its superconductivity similar to the A-phase of superfluid ³He [3,4]. For a long time, chiral *p*-wave superconductivity with spin-triplet pairing has been considered to best describe the majority of experimental studies [5,6], although the absence of detectable edge currents [7] and the constant Knight-shift observed for fields perpendicular to the Ru layers [8] were not easily explained in this scenario [9]. Further insight was gained from experiments performed under large uniaxial strain that revealed a considerable enhancement of the superconducting transition temperature by more than a factor 2 [10,11], similar to the enhancement in the eutectic crystals [6]. However, the breaking of the fourfold axis should split the superconducting transition of the chiral state in contradiction with a single anomaly appearing in the specific heat under strain [12]. Furthermore, the strain dependence of the transition temperature close to zero strain is flat [10,13], whereas one expects a linear dependence for the chiral state.

The picture of chiral *p*-wave superconductivity was fully shaken when the two experiments yielding the strongest support for triplet pairing [14,15] were revised. The new studies of the Knight shift in NMR [16,17] and those of the polarized neutron diffraction [18] reveal an unambiguous drop of the

electronic susceptibility that is inconsistent with spin-triplet pairs parallel to Ru layers. Since then, numerous proposals for the superconducting state were made mostly invoking some *d*-wave state, and the discussion of the superconducting pairing has become very active [19–26]. The observations of broken time-reversal symmetry in muon spin relaxation experiments [27,28] and in measurements of the magneto-optical Kerr effect [29] may require interpretations other than the chiral *p*-wave scenario. Many theories discuss a superconducting state with a complex combination of components [19–25].

Assuming a simple boson-mediated pairing following BCS theory, phonons and magnetic fluctuations or a combination of both [30] can be relevant. There are anomalies in the phonon dispersion that could be fingerprints of electron phonon coupling [31,32]. The phonon mode that describes the rotation of the RuO₆ octahedra around the *c* axis exhibits an anomalous temperature dependence and severe broadening [31]. This mode can be associated with the structural phase transition and with the shift of the van Hove singularity in the γ band through the Fermi level. Both effects occur upon small Ca substitution [33,34]. In addition, the Ru-O bond-stretching modes that exhibit an anomalous downward dispersion in many oxides with perovskite-related structure [35] exhibit an anomalous dispersion in Sr₂RuO₄ as well [32]. Comparing the first-principles calculated [36] and measured [32] phonon dispersion in Sr₂RuO₄, the agreement is worst for these longitudinal bond-stretching modes, which exhibit a flatter dispersion indicating better screening compared to the density functional theory (DFT) calculations. Note, however, that perovskite oxides close to charge ordering exhibit a much stronger renormalization of the zone-boundary modes with breathing character that is frequently labeled overscreening [35,37].

*jenni@ph2.uni-koeln.de

†braden@ph2.uni-koeln.de

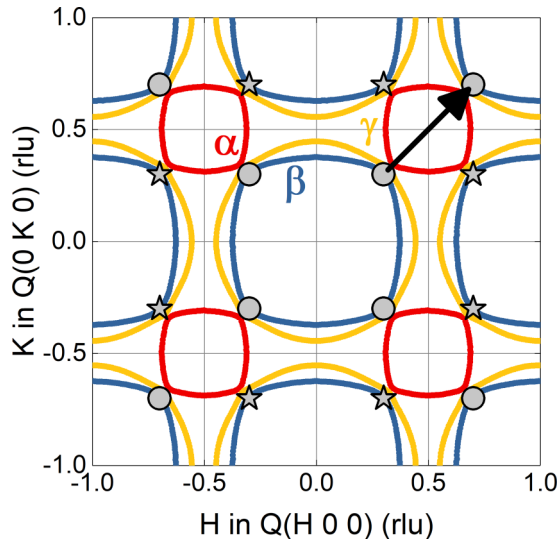


FIG. 1. Fermi surface of Sr_2RuO_4 for $k_z = 0$. The bands are based on LDA+SO calculations from [60] and marked by different colors. The black arrow represents the dominant nesting vector between the one-dimensional sheets α (red) and β (blue). The incommensurate positions of the in-plane nesting signal are marked by different symbols. The circles represent the crystallographically equivalent positions $(\pm 0.3, \pm 0.3)$ and $(\pm 0.7, \pm 0.7)$. The positions $(\pm 0.3, \pm 0.7)$ and $(\pm 0.7, \pm 0.3)$ shown by stars are equivalent to those on the diagonals only in a purely two-dimensional picture, because $(1\ 0\ 0)$ is not an allowed Bragg peak in the body-centered lattice.

On the other side there is clear evidence for strong magnetic fluctuations deduced from NMR [38] and inelastic neutron scattering (INS) experiments [39–45]. The dominating magnetic signal is incommensurate and stems from nesting in the one-dimensional bands associated with d_{xz} and d_{yz} orbitals; see Fig. 1. The relevance of this instability toward an incommensurate spin-density wave (SDW) is underlined by the observation of static magnetic order emerging at this \mathbf{q} position in reciprocal space for minor substitution of Ru by Ti [46] or of Sr by Ca [47,48]. A repulsive impurity potential was recently proposed to form the nucleation center for the magnetic ordering that should strongly couple to charge currents [49]. Furthermore, the temperature dependence of these incommensurate magnetic fluctuations in pure Sr_2RuO_4 agrees with a closeness to a quantum critical point [40]. These nesting-induced magnetic fluctuations can easily be explained by DFT calculations using the random phase approximations (RPA) [50], but their relevance for the superconducting pairing remains controversial [51]. Inelastic neutron scattering in the superconducting state can exclude the opening of a large gap for these nesting-driven fluctuations [52]. Since magnetic excitations are particle-hole excitations, one expects in the simplest isotropic case a magnetic gap comparable to twice the superconducting one, which can be safely excluded. However, the anisotropy of the gap function and interactions can strongly modify the magnetic response in the superconducting state. A more recent time-of-flight (TOF) inelastic neutron scattering experiment confirms the absence of a large gap but reports weak evidence for suppression of spectral weight

at very low energies [53]. This experiment also claims the occurrence of a spin resonance mode at the nesting position with a finite perpendicular wave-vector component, which would point to an essential modulation of the superconducting gap perpendicular to the RuO_2 layers but which is inconsistent with the results of this work.

In addition to the incommensurate nesting-induced fluctuations, macroscopic susceptibility [54], NMR [38,55], and also polarized inelastic neutron scattering experiments [42,45] reveal the existence of magnetic fluctuations centered at the origin of the Brillouin zone, which typically can be associated with ferromagnetism. Furthermore, a small concentration of Co doping can lead to static short-range ferromagnetic order [56]. All techniques find almost temperature-independent quasiferromagnetic excitations in pure Sr_2RuO_4 . This ferromagnetic response agrees qualitatively with a recent dynamical mean-field theory (DMFT) analysis of magnetic fluctuations [57], which finds essentially local magnetic fluctuations superposed on the well-known nesting signal. However, the neutron data disagree with a fully local character as they show a finite q dependence [45]. The quasiferromagnetic fluctuations also disagree with the expectations for a nearly ferromagnetic system that exhibits paramagnon scattering [45,58]. SrRuO_3 clearly exhibits such paramagnon scattering with its well-defined structure in q and energy space [59].

Here we present additional neutron scattering experiments on the magnetic fluctuations in Sr_2RuO_4 , which focus on several aspects that are particularly relevant for the superconducting pairing mechanism involving magnetic fluctuations or for the general understanding of magnetic excitations in a strongly correlated electron system. We discuss the possibility of important out-of-plane dispersion in the magnetic response in the superconducting and normal states, the shape of nesting scattering away from the peak position, and the nonlocal character of the quasiferromagnetic response.

II. EXPERIMENT

INS experiments were carried out on the ThALES [61,62] and IN20 [63] triple-axis spectrometers (TAS) at the Institut Laue Langevin and on the LET [64] TOF spectrometer at the ISIS Neutron and Muon Source. We used an assembly of 12 Sr_2RuO_4 crystals with a total volume of 2.2 cm^3 in all experiments. At Kyoto University, the crystals were grown using the floating zone method, and similar crystals were studied in many experiments [5,6]. The crystal assembly was oriented in the $[100]/[010]$ scattering plane (corresponding to a vertical c axis) to study the in-plane physics of the Ru layers. Additionally, with the instruments ThALES and LET it was possible to access parts of the q space perpendicular to the plane, which enables an analysis of the out-of-plane dispersion of the magnetic response. To conduct experiments inside the superconducting phase, a dilution refrigerator was used, reaching a temperature of $\sim 200\text{ mK}$, well below the transition temperature of $\sim 1.5\text{ K}$. ThALES and LET are operating with a cold neutron source providing the energy resolution to study the magnetic response down to $\sim 200\text{ }\mu\text{eV}$. The TOF spectrometer LET records data simultaneously with four different values of the incidental energies, E_i , and

resolutions, while the energy resolution of the TAS ThALES is determined by the chosen final neutron wave vector k_f of 1.57 \AA^{-1} combined with the collimations. On ThALES the best intensity-to-background ratio was achieved by using a Si(111) monochromator and PG(002) analyzer combined with a radial collimator in front of the analyzer for further background reduction. The same configuration was also used in an earlier study [52].

A polarized neutron scattering experiment was performed on the thermal TAS IN20 using Heusler crystals as monochromator and analyzer. A spin flipper in front of the analyzer enabled the polarization analysis. The scans were performed with a fixed final momentum of $k_f = 4.1 \text{ \AA}^{-1}$, where the graphite filter in front of the analyzer cuts higher-order contaminations. Longitudinal polarization analysis was performed with a set of Helmholtz coils.

III. RESULTS AND DISCUSSION

A. q dependence of fluctuations associated with nesting

The TOF technique enables an imaging of the complete Q - E space, which gives insight on the distribution of scattering intensity in reciprocal space. Throughout the paper, the scattering vector, $\mathbf{Q} = (H, K, L)$, and the propagation vector in the first Brillouin zone, $\mathbf{q} = (q_h, q_k, q_l)$, are given in reciprocal-lattice units (rlu). We mostly consider only the planar wave vector $\mathbf{Q}_{2d} = (H, K)$ projection. Figure 2 shows the inelastic scattering plotted against the H, K components of the scattering vector in the superconducting phase. The four different panels display sections of the two-dimensional (H, K) plane for different incident energies and hence different resolutions. The intensities are fully integrated along the energy transfer (depending on the incident energy) and along the out-of-plane component of the scattering vector, $-0.7 < L < 0.7$. The high scattering intensities at the incommensurate positions $(\pm 0.3, 0.3)$, $(\pm 0.3, 0.7)$, and $(\pm 0.7, 0.7)$ are clearly visible, arising from the well-known antiferromagnetic fluctuations [39–41,43,44]. Additionally, there are ridges of scattering intensities connecting these positions in the $[\xi, 0]$ and $[0, \xi]$ directions that were first reported in [43,44]. The arc visible in Fig. 2(d) connecting $(-0.3, 0.3)$ and $(0.3, 0.3)$ is a spurious signal; it does not appear for the other incidental energies.

Neglecting electronic dispersion perpendicular to the planes and assuming an idealized scheme of flat one-dimensional bands originating from the d_{xz} and d_{yz} orbitals, one expects nesting-induced magnetic excitations for any two-dimensional vector $\mathbf{Q}_{2d} = (\mathbf{0.3}, \xi)$ and $(\xi, \mathbf{0.3})$ and accordingly a peak at $(0.3, 0.3)$ [50]. The peaks clearly dominate but the ridges are also detectable—mostly for the positions connecting the nesting peaks, i.e., $0.3 < \xi < 0.7$. This is in accordance with the calculation of the bare susceptibility, which shows an enhanced signal only between the peaks, i.e., for the paths from $(0.3, 0.3)$ to $(0.7, 0.3)$ [50].

To analyze the ridge scattering and the anisotropy of the incommensurate signals in detail, Fig. 3(a) shows one-dimensional cuts along the ridge in the $[\xi, 0]$ direction calculated from the data taken with $E_i = 14.13 \text{ meV}$ [Fig. 2(a)]. By subtracting the background obtained from the

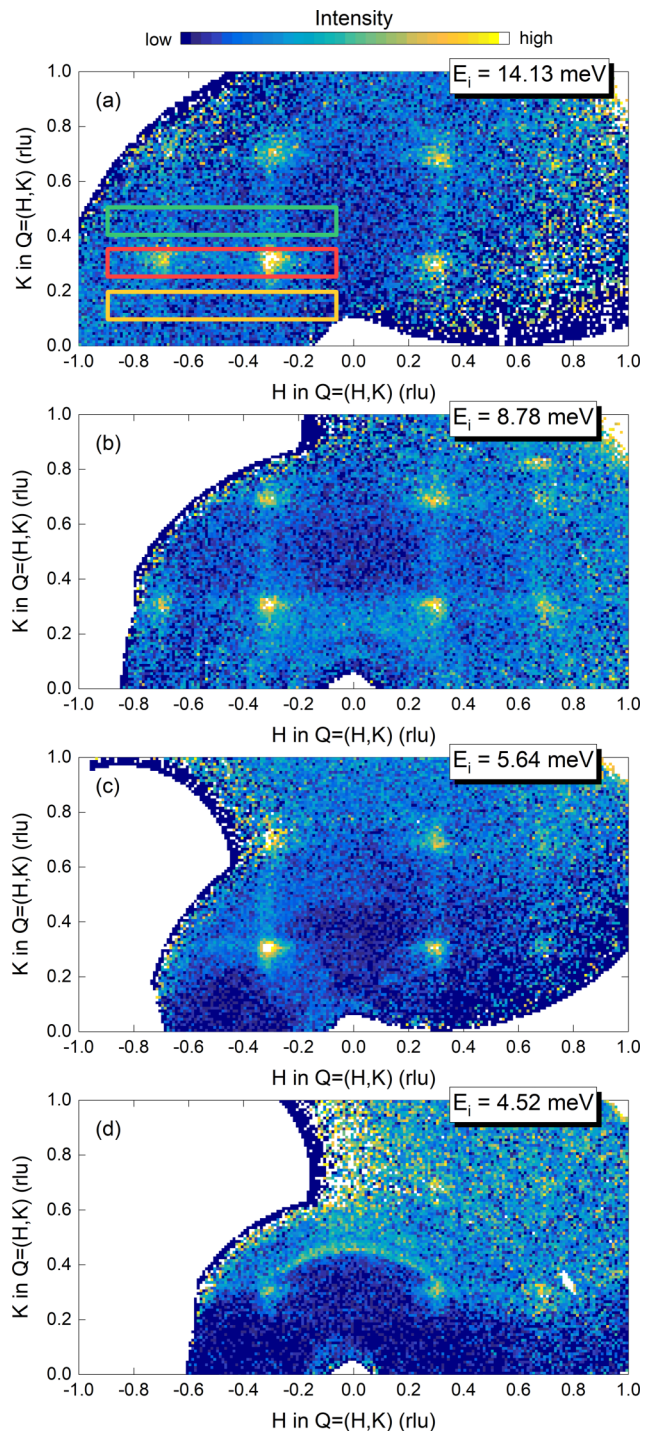


FIG. 2. In-plane scattering in the superconducting phase ($T = 0.2 \text{ K}$). The TOF data at four different incident energies display the magnetic scattering distribution in the ab plane. The intense signal at the incommensurate positions $(0.3, 0.3)$, $(0.7, 0.7)$, and $(0.3, 0.7)$ is visible for all E_i . Additionally, there is magnetic scattering between the incommensurate positions in the $[\xi, 0]$ and $[0, \xi]$ directions, respectively. To increase the statistics, the data are integrated over the maximum L range of $[-0.7, 0.7]$ and the full E range depending on the incident energy ($1.75 < E < 10$ for $E_i = 14.13 \text{ meV}$, $0.8 < E < 6.7$ for $E_i = 8.78 \text{ meV}$, $0.7 < E < 4.5$ for $E_i = 5.64 \text{ meV}$, and $0.5 < E < 3.5$ for $E_i = 4.52 \text{ meV}$). The overlaid rectangles in (a) represent the integration area of the one-dimensional cuts displayed in Figs. 3(a)–3(c).

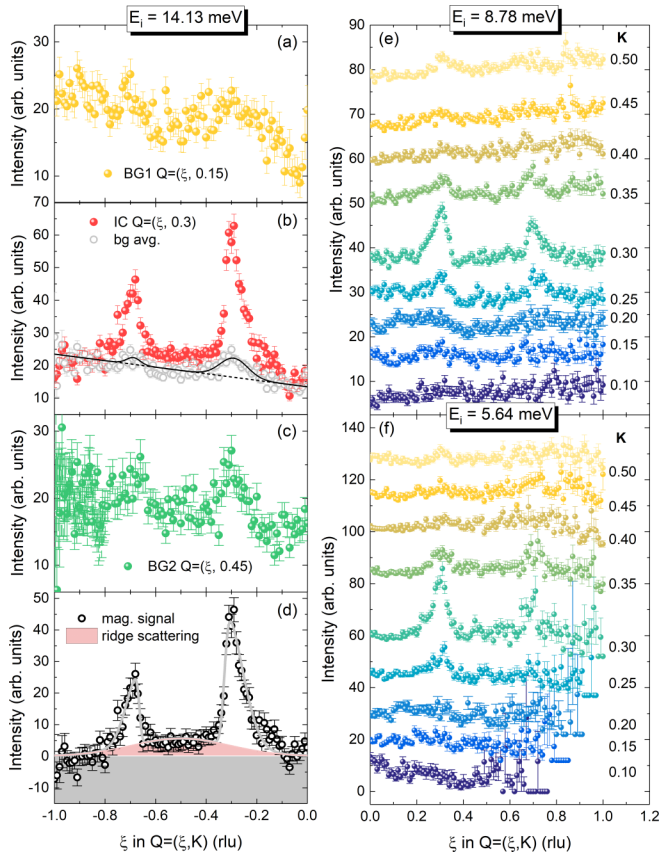


FIG. 3. Magnetic scattering along the connection of the incommensurate positions. Parts (a)–(c) show one-dimensional cuts from Fig. 2(a) along the (ξ, K) paths for $K = 0.15$ (a), 0.3 (b), and 0.45 (c). The background at both sides of the incommensurate positions is displayed in (a) and (c) [represented by the same colored rectangles as in (a)]. An averaged background is formed from both (gray open circles) and fitted with a linear contribution and two Gaussians (black solid line). This is compared to the incommensurate signal in (b). In (d) the linear background contribution (black dashed line) is subtracted, and the signal along the $[\xi, 0]$ direction is fitted with two skew Gaussians for the incommensurate signal and a broad Gaussian fixed at $\xi = 0.5$ (red area), taking into account the ridge scattering. Parts (e) and (f) represent one-dimensional cuts for different K and two different incident energies 8.78 and 5.64 meV taken from Figs. 2(b) and 2(c). The integration range in the $[0, \xi]$ direction is ± 0.025 around the K value, and the scans are shifted vertically for better visibility.

average of $(\xi, 0.15)$ and $(\xi, 0.45)$, shown in Figs. 3(b) and 3(c), respectively, we isolate the signal along the line $(\xi, 0.3)$ shown in Fig. 3(d). The ridge scattering is mainly detectable between the peaks at the incommensurate positions, as it is visible in the two one-dimensional cuts representing the background parallel to the ridge on both sides [Figs. 3(b) and 3(c)]. While the $(\xi, 0.15)$ cut exhibits only a weak signal around $(-0.3, 0.15)$, the $(\xi, 0.45)$ cut shows clearly two peaks at the $(-0.7, 0.45)$ and $(-0.3, 0.45)$ positions representing the ridges in the $[0, \xi]$ direction. The rounding of the one-dimensional Fermi-surface sheets suppresses the susceptibility at $(0.3, \xi)$ with ξ lower than 0.3 , but this suppression is not abrupt. Besides the ridge scattering, we may also confirm

the pronounced asymmetry of the nesting peak with a shoulder near $(0.25, 0.3)$ and equivalent positions. This shoulder was reported in [40] and was also found in the full RPA calculations.

The asymmetry of the nesting peaks and the ridge scattering between the incommensurate positions can also be seen in the data of lower incident energies [see Figs. 3(e) and 3(f)]. The one-dimensional cuts for different K values confirm the asymmetric shape of the nesting peaks. A thorough analysis of the pure magnetic signal as in the case of $E_i = 14.13$ meV is not possible due to uncertainty in the background. Furthermore, the ridge scattering is less pronounced in the data obtained with lower incident energies, which indicates a higher characteristic energy of the ridge scattering. This further explains why the much weaker scattering in the ridges has not been detected in early TAS studies [39–41].

B. Search for a gap opening or a resonance mode below T_c

The opening of a superconductivity-induced gap in the spectrum of magnetic fluctuations would have a strong impact on the discussion of the superconducting character in Sr_2RuO_4 . Previous INS experiments using a TAS revealed the clear absence of a large gap at the nesting position [52], whereas a recent TOF experiment reports a tiny gap, although the statistics remained very poor [53]. Studying the magnetic response of Sr_2RuO_4 in its superconducting phase by INS is challenging, because one needs to focus on small energies of the order of 0.2 – 0.5 meV. At these energies, the signal in the normal state is at least one order of magnitude below its maximum strength at 6 meV, and the required high-energy resolution further suppresses statistics. Figure 4 presents the TOF data obtained with $E_i = 3$ meV by calculating the energy dependence at the nesting position integrated over all L values. The full L integration is needed to enhance the statistics. In Figs. 4(a) and 4(b), we compare the raw data for both temperatures with the background signal. In Fig. 4(c), the background-subtracted magnetic response in the superconducting phase is compared to that in the normal phase. There is no evidence for the opening of a gap within the statistics of this TOF experiment. Also, a resonance at a finite energy cannot be detected. Admittedly, the statistics of these TOF data is too poor to detect small signals or their suppression.

Following the claim of Iida *et al.* [53], the TOF data are also analyzed in terms of a possible resonance mode appearing at a finite value of the L component, i.e., at $(0.3, 0.3, L)$. Therefore, the L dependence of the magnetic signal at $(0.3, 0.3, L)$ is determined by background subtraction and compared for the two temperatures (see Fig. 5). The different panels represent the energy ranges from Ref. [53], where a resonance appearing at 0.56 meV is proposed for $L = 0.5$. In our data shown in Fig. 5(b), there is no difference visible between superconducting and normal phase at $L = \pm 0.5$.

To study the low-energy response and its L dependence in more detail and with better statistics, the TAS is better suited since measurements can be focused on single \mathbf{Q} , \mathbf{E} points. Using ThALES and its high flux and energy resolution, constant- \mathbf{Q} scans at the incommensurate position $(0.3, 0.7, L)$ with $L = 0, 0.25$, and 0.5 were measured to investigate the L dependence of the low-energy response (see Fig. 6). This incommensurate position was chosen due to a better

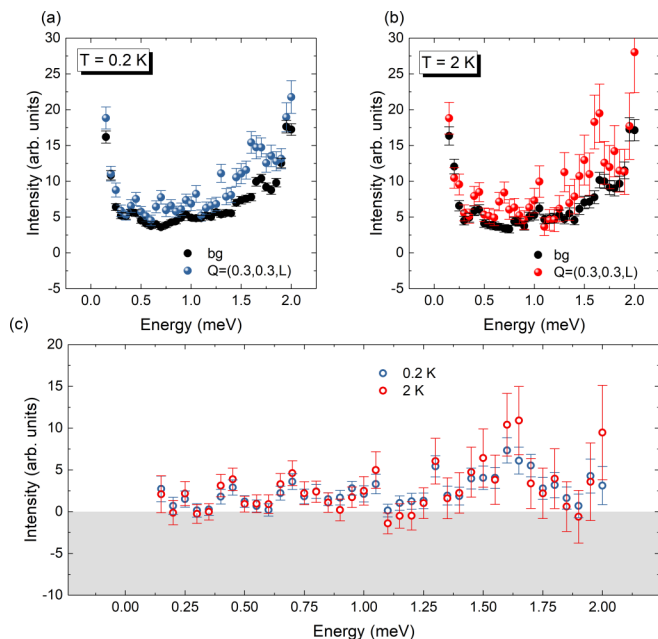


FIG. 4. Low-energy dependence of the incommensurate signal below and above the superconducting transition extracted from TOF data. Parts (a) and (b) display the energy scans at $q = (0.3, 0.3)$ below ($T = 0.2$ K) and above ($T = 2$ K) the superconducting phase transition. The background in both panels is derived from the constant Q cut at $(0.09, 0.41)$ for both temperatures ($|Q_{IC}| = |Q_{bg}|$). To increase statistics, the TOF data with an incidental energy of 3 meV are fully integrated over L (range $[-0.7, 0.7]$) and symmetrized by folding in q space at $(0.3, 0.7)$ along the $(1, -1, 0)$ plane. The H and K components are integrated with the range $[0.25, 0.35]$. (c) The background subtraction and Bose factor correction yield the pure magnetic response at low energies, which is compared inside and outside the superconducting phase.

signal-to-noise ratio compared to $(0.3, 0.3, L)$ and because the larger $|Q|$ value allows one to reach finite L values by tilting the cryostat. Similar to Figs. 4(a) and 4(b), the raw data for two temperatures are shown in Figs. 6(a)–6(c). The background was measured by rotating ω by 20° for each L value and then combining all three backgrounds to an average. For all L values, the intensity of the incommensurate signal increases approximately linearly for small energies, following the established single relaxor behavior. Comparing the two temperatures, there is no difference noticeable for any L value down to the energy resolution. Especially around 0.56 meV, where Iida *et al.* [53] propose a resonance at the incommensurate position $(0.3, 0.3, 0.5)$, the two temperatures yield comparable signals. It should be noted here that while the incommensurate positions $(0.3, 0.3, 0)$ and $(0.3, 0.7, 0)$ are crystallographically not equivalent, both positions become equivalent with the L component 0.5; see Fig. 1. Therefore, the data taken at $(0.3, 0.3, 0.5)$ and $(0.7, 0.3, 0.5)$ can be compared. To emphasize the absence of a resonance mode around 0.56 meV, the data from Fig. 6 are plotted with a larger energy binning to further increase the statistics (see Fig. 7, which also indicates the broad energy integration used in [53]). There is no significant deviation from the general linear behavior for any L value at low temperatures detectable. Iida *et al.*

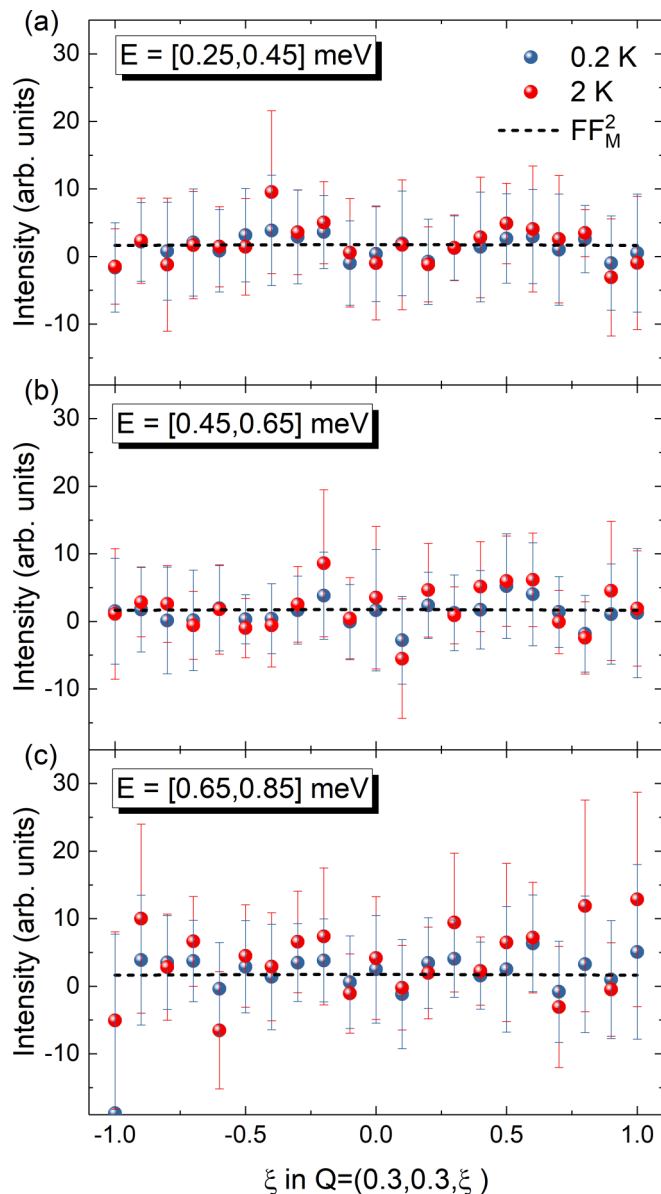


FIG. 5. L dependence of the incommensurate signal at low energies extracted from TOF data. Constant E cuts with an integration width of 0.2 meV at the incommensurate position $(0.3, 0.3, L)$ were adjusted for the measured background at the same energy at $(0.09, 0.41, L)$ and corrected for the Bose factor. The L dependence of the magnetic response in the superconducting phase (blue) is compared to the normal phase (red). Additionally, the square of the Ru^{1+} form factor is depicted in each panel (black dashed line). There is no evidence for a peak at $L = 0.5$.

[53] report a signal increase of $\sim 60\%$ for $L = 0.5$ in the superconducting phase, which clearly is incompatible with our data that offer higher statistics.

Since no L dependence of the magnetic low-energy response can be established (Figs. 6 and 7), we merge the data and compare them with the previously published low-energy dependence of the incommensurate signal [52] (see Fig. 8). The new experiments below T_c fully confirm that the nesting excitations in Sr_2RuO_4 do not exhibit a large gap, i.e., a magnetic gap comparable to twice the superconducting one.

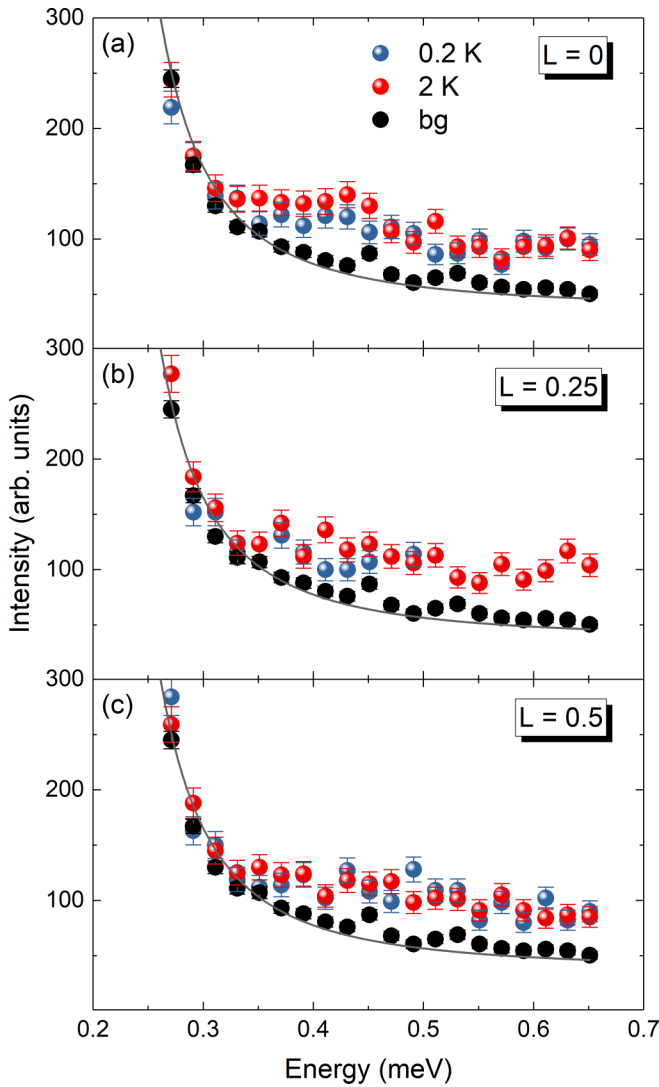


FIG. 6. L dependence of the incommensurate signal at low energies extracted from TAS data. The constant- q scans were conducted at the incommensurate positions $(0.3, 0.7, L)$ with $L = 0, 0.25$, and 0.5 in the superconducting and normal phase. The background for each L is measured after ω rotation of 20° , thus keeping $|q|$ constant, and later averaged for all scans, yielding the presented background (black circles) and its fit (gray). The intensity is normalized with 1 980 000 monitor counts, which corresponds to a measuring time of about 15 min per point.

Combining all the previous and new data, there is, however, some weak evidence for the suppression of magnetic scattering at very low energies below 0.25 meV. With the neutron instrumentation of today it seems very difficult to further characterize the suppression of the small signal at such low energy.

For the previously assumed superconducting state, detailed theoretical analyses of the magnetic response were reported [51], but concerning the more recently proposed superconducting symmetries [19–26], such investigations are lacking. The $d_{x^2-y^2}$ state deduced from quasiparticle interference imaging [26] exhibits nodes at Fermi-surface positions that are connected through the nesting vector. This implies that even

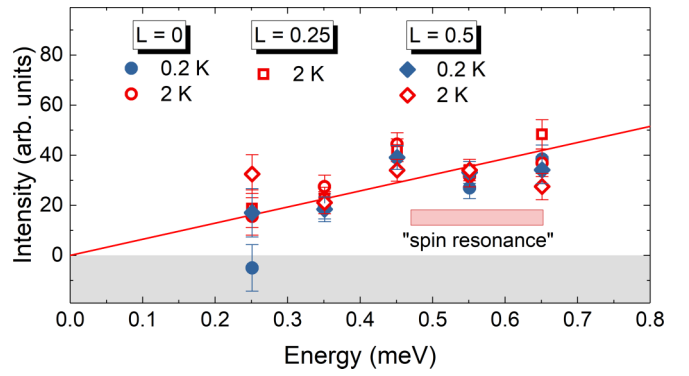


FIG. 7. Comparison of the background-free incommensurate signal $Q = (0.3, 0.7, L)$ for different L values and temperatures. The compared data originate from the constant- q scans shown in Fig. 6. The binning is increased to $\Delta E = 0.1$ meV, which yields better statistics. A linear fit (red line) provides a guide to the eye. The energy range of the proposed spin resonance [53] is indicated by the red box.

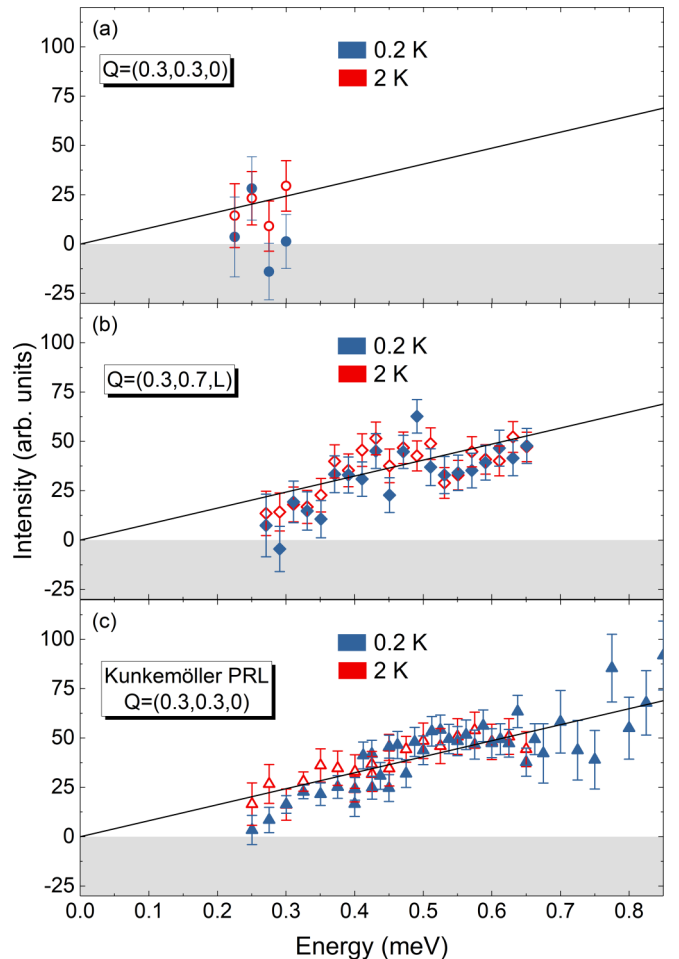


FIG. 8. Comparison of the energy dependence of the incommensurate signal with former published data from [52] (labeled Kunkemöller PRL). Background-corrected data recorded at $(0.3, 0.3, 0)$ (circles) is given in panel (a); the background free signal at $(0.3, 0.7)$ is averaged over all L values for both temperatures (diamonds), panel (b), and the incommensurate signal reported in [52] (triangles) is shown in (c). Data were corrected for the Bose and magnetic form factors.

at very low energies, the nesting-induced excitations are not fully suppressed in such a $d_{x^2-y^2}$ superconducting state, in agreement with the experimental absence of a large gap in the nesting spectrum [52]. Within the $d_{x^2-y^2}$ superconducting state, the nesting vector also connects Fermi-surface regions with maximum and minimum gap values, and it connects either two regions of the β sheet or one β region with an α region. Therefore, the conditions for a spin-resonance mode are more complex and less favorable than in the case of the FeAs-based superconductors, where the s^{+-} superconducting symmetry and the nesting magnetic fluctuations perfectly match each other [65].

C. Shape of the quasiferromagnetic fluctuations

The polarization analysis of inelastic neutron scattering provides the separation of the magnetic contribution from any other scattering contribution. It is therefore possible to identify a tiny magnetic response that is little structured in \mathbf{q} space. This technique was used to detect quasiferromagnetic fluctuations and to determine their strength in comparison to the incommensurate fluctuations in Sr_2RuO_4 [45]. We wished to extend this study focusing on the \mathbf{q} dependence of the magnetic quasiferromagnetic response. Recent DMFT calculations [57] find evidence for local fluctuations superposing the well-established nesting excitations, which agree qualitatively with the experimental quasiferromagnetic signal. However, while the neutron experiments indicate a finite suppression of the quasiferromagnetic response toward the boundaries of the Brillouin zone, the DMFT calculation obtains an essentially local feature without such a \mathbf{q} dependence.

The polarized neutron study was performed on the thermal TAS IN20, and the results are shown in Fig. 9. An example of the raw data with different spin channels that are needed for the polarization analysis is given in Fig. 9(a), where a diagonal constant energy scan at 8 meV, reaching from the zone boundary (0.5,0.5) over the incommensurate position (0.7,0.3) to the zone center (1,0), is shown. The x, y, z indices refer to the common coordinate system used in neutron polarization analysis with respect to the scattering vector \mathbf{Q} [45]. The three spin-flip channels $\text{SF}_x, \text{SF}_y,$ and SF_z clearly exhibit a maximum at the incommensurate position. While SF_y and SF_z exhibit comparable amplitudes, SF_x carries the doubled intensity as it senses both magnetic components perpendicular to the scattering vector. There is an enhancement of magnetic excitations polarized along the c direction that can be seen in the stronger SF_y and that was studied in Ref. [42]. Assuming a polarization-independent background, $2I(\text{SF}_x) - I(\text{SF}_y) - I(\text{SF}_z)$ yields the background-free magnetic signal; see the discussion in Ref. [45].

Figure 9(b) displays the magnetic signal, corrected for the Bose factor, i.e., the imaginary part of the susceptibility, for different energies and temperatures. The data agree well with the results for 8 meV and 1.6 K presented in [45]. Additionally, the data at 290 K indicate a significant drop of the incommensurate nesting signal, which, however, is still finite and clearly observable. The temperature dependence of the incommensurate signal was first discussed in Ref. [39], where the neutron scattering results are compared to the NMR results from Ref. [38]. The incommensurate

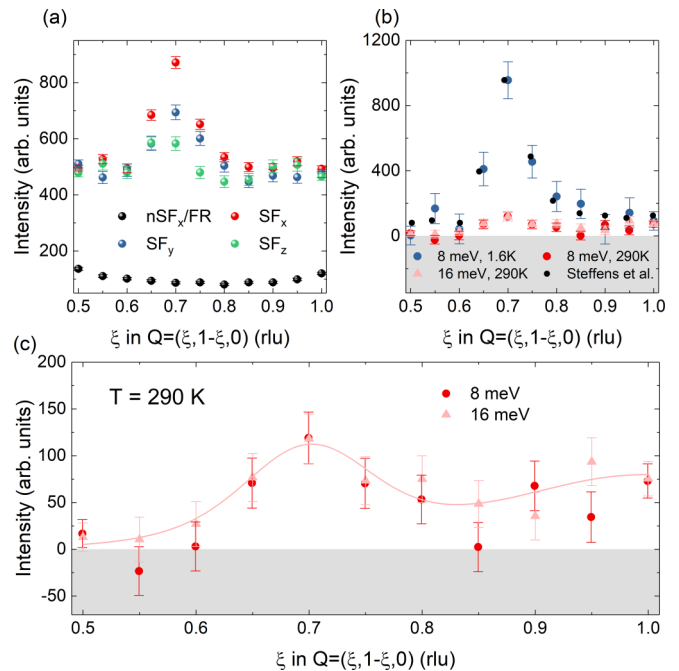


FIG. 9. Polarized neutron analysis of the scattering along the diagonal of the first Brillouin zone. (a) An example of constant energy scans for all three spin-flip channels displays the increased scattering at the incommensurate position (0.7,0.3,0) at 8 meV and 1.6 K. The polarization analysis of all channels yields the purely magnetic scattering signal displayed in (b) for different energies and temperatures. The black circles represent data of the previously reported polarization analysis, taken from [45]. This dataset was also measured at 8 meV and 1.6 K. (c) The magnetic signal at 290 K can be described by the susceptibility model used in [45] (light red line). The intensity in (a) is normalized with 7 800 000 monitor counts, which corresponds to a measuring time of about 20 min per point.

signal was found to strongly decrease with increasing temperature up to room temperature, while the ferromagnetic component of the NMR is nearly temperature-independent. Also, the previous polarized neutron experiment found the quasiferromagnetic contribution to be almost identical at 1.6 and 160 K [45]. As indicated in Fig. 9(b), the quasiferromagnetic signal does not change up to 290 K, thus the peak heights of incommensurate and quasiferromagnetic contributions are comparable at ambient temperature. Taking the much broader q shape of the quasiferromagnetic excitations into account, the q -integrated spectral weight of the latter clearly dominates. Around room temperature, therefore, the quasiferromagnetic fluctuations have a larger impact on any integrating processes such as electron scattering. The quasiferromagnetic fluctuations at 290 K, however, do not exhibit a local character as the signal is significantly reduced at the antiferromagnetic zone boundary (0.5,0.5,0) [Fig. 9(c)]. This confirms the conclusion of Steffens *et al.* [45] that the quasiferromagnetic fluctuations are sharper in q space than expected from the calculations. Also, at the other zone boundary (0.5,0,0) there is no significant magnetic signal detectable (see Fig. 10).

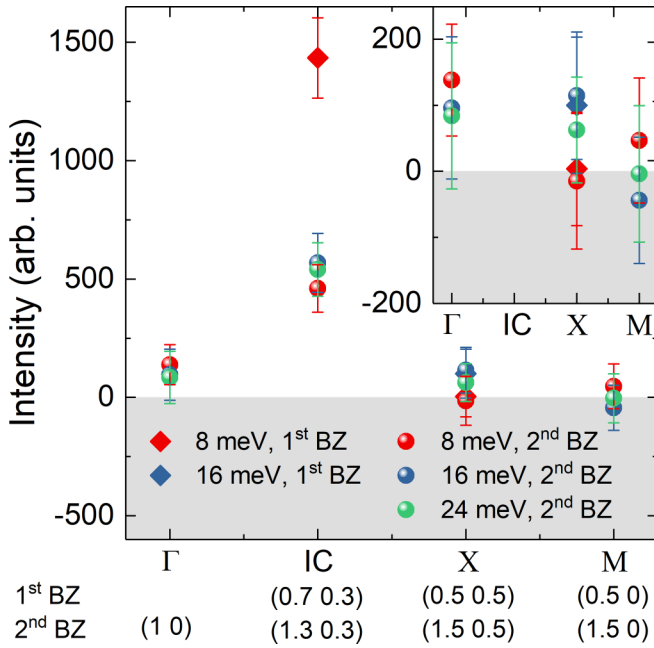


FIG. 10. Comparison of magnetic scattering ($T = 1.6$ K) at prominent points in k -space with $L = 0$. The magnetic signal was extracted using the polarization analysis $[2I(\text{SF}_x) - I(\text{SF}_y) - I(\text{SF}_z)]$ and is displayed for the points in the Brillouin zone and different energies: Γ point, the incommensurate position, and the different zone boundaries X and M. The inset magnifies the intensity region around zero.

IV. CONCLUSION

Polarized and unpolarized neutron scattering experiments were performed to study several aspects of the magnetic fluctuations in Sr_2RuO_4 that are particularly relevant for a

possible superconducting pairing scenario. The TOF instrument LET yields full mapping of the excitations and reveals the well-studied incommensurate fluctuations at $(0.3, 0.3)$ in two-dimensional reciprocal space. There is also ridge scattering at $(0.3, \xi)$ reflecting the one-dimensional character of the d_{xz} and d_{yz} bands, as first reported in Refs. [43,44]. These ridges are stronger between the four peaks surrounding $(0.5, 0.5)$, i.e., for $\xi > 0.3$, but the suppression of the signal at smaller ξ is gradual. The TOF data confirm the pronounced asymmetry of the nesting peaks. Concerning the study of the nesting fluctuations at very low energy in the superconducting phase, TAS experiments yield higher statistics due to the possibility to focus the experiment on the particular position in \mathbf{Q}, E space. Data taken at different out-of-plane components of the scattering vector exclude a sizable resonance mode emerging at $L = 0.5$ in the superconducting phase. Only by combining the results of several experiments can one obtain some evidence for the suppression of spectral weight at very low energies.

With neutron polarization analysis, the magnetic excitations were further characterized at 290 K. The incommensurate nesting signal is strongly reduced but still visible, while the quasiferromagnetic contribution is almost unchanged. At this temperature, there is a suppression of this quasiferromagnetic scattering at the Brillouin-zone boundaries, which underlines that this response is not fully local.

ACKNOWLEDGMENTS

We acknowledge stimulating discussions with I. Eremin. This work was funded by the Deutsche Forschungsgemeinschaft (DFG, German Research Foundation)–Project No. 277146847–CRC 1238, project B04, the JSPS KAKENHI Grants No. JP15H05852 and No. JP17H06136, and the JSPS core-to-core Program No. JPJSCCA20170002.

- [1] Y. Maeno, H. Hashimoto, K. Yoshida, S. Nishizaki, T. Fujita, J. G. Bednorz, and F. Lichtenberg, Superconductivity in a layered perovskite without copper, *Nature (London)* **372**, 532 (1994).
- [2] G. Koster, L. Klein, W. Siemons, G. Rijnders, J. S. Dodge, C. B. Eom, D. H. A. Blank, and M. R. Beasley, Structure, physical properties, and applications of SrRuO_3 thin films, *Rev. Mod. Phys.* **84**, 253 (2012).
- [3] G. Baskaran, Why is Sr_2RuO_4 not a high T_c superconductor? Electron correlation, Hund's coupling and p-wave instability, *Phys. B* **223**, 490 (1996).
- [4] T. M. Rice and M. Sigrist, Sr_2RuO_4 : an electronic analogue of ^3He ?, *J. Phys. Condens. Matter* **7**, L643 (1995).
- [5] A. P. Mackenzie and Y. Maeno, The superconductivity of Sr_2RuO_4 and the physics of spin-triplet pairing, *Rev. Mod. Phys.* **75**, 657 (2003).
- [6] Y. Maeno, S. Kittaka, T. Nomura, S. Yonezawa, and K. Ishida, Evaluation of spin-triplet superconductivity in Sr_2RuO_4 , *J. Phys. Soc. Jpn.* **81**, 011009 (2012).
- [7] C. W. Hicks, J. R. Kirtley, T. M. Lippman, N. C. Koshnick, M. E. Huber, Y. Maeno, W. M. Yuhasz, M. B. Maple, and K. A. Moler, Limits on superconductivity-related magnetization in Sr_2RuO_4 and $\text{PrOs}_4\text{Sb}_{12}$ from scanning SQUID microscopy, *Phys. Rev. B* **81**, 214501 (2010).
- [8] H. Murakawa, K. Ishida, K. Kitagawa, Z. Q. Mao, and Y. Maeno, Measurement of the ^{101}Ru -Knight Shift of Superconducting Sr_2RuO_4 in a Parallel Magnetic Field, *Phys. Rev. Lett.* **93**, 167004 (2004).
- [9] C. Kallin, Chiral p-wave order in Sr_2RuO_4 , *Rep. Prog. Phys.* **75**, 042501 (2012).
- [10] C. W. Hicks, D. O. Brodsky, E. A. Yelland, A. S. Gibbs, J. A. N. Bruin, M. E. Barber, S. D. Edkins, K. Nishimura, S. Yonezawa, Y. Maeno, and A. P. Mackenzie, Strong increase of T_c of Sr_2RuO_4 under both tensile and compressive strain, *Science* **344**, 283 (2014).
- [11] A. Steppke, L. Zhao, M. E. Barber, T. Scaffidi, F. Jerzembeck, H. Rosner, A. S. Gibbs, Y. Maeno, S. H. Simon, A. P. Mackenzie, and C. W. Hicks, Strong peak in T_c of Sr_2RuO_4 under uniaxial pressure, *Science* **355**, 6321 (2017).
- [12] Y. S. Li, N. Kikugawa, D. A. Sokolov, F. Jerzembeck, A. S. Gibbs, Y. Maeno, C. W. Hicks, M. Nicklas, and A. P. Mackenzie, High sensitivity heat capacity measurements on Sr_2RuO_4 under uniaxial pressure, *Proc. Natl. Acad. Sci.* **118**, e2020492118 (2021).

- [13] M. E. Barber, F. Lechermann, S. V. Streltsov, S. L. Skornyakov, S. Ghosh, B. J. Ramshaw, N. Kikugawa, D. A. Sokolov, A. P. Mackenzie, C. W. Hicks, and I. I. Mazin, Role of correlations in determining the Van Hove strain in Sr_2RuO_4 , *Phys. Rev. B* **100**, 245139 (2019).
- [14] K. Ishida, H. Mukuda, Y. Kitaoka, K. Asayama, Z. Q. Mao, Y. Mori, and Y. Maeno, Spin-triplet superconductivity in Sr_2RuO_4 identified by ^{17}O Knight shift, *Nature (London)* **396**, 658 (1998).
- [15] J. A. Duffy, S. M. Hayden, Y. Maeno, Z. Mao, J. Kulda, and G. J. McIntyre, Polarized-Neutron Scattering Study of the Cooper-Pair Moment in Sr_2RuO_4 , *Phys. Rev. Lett.* **85**, 5412 (2000).
- [16] A. Pustogow, Y. Luo, A. Chronister, Y. S. Su, D. A. Sokolov, F. Jerzembeck, A. P. Mackenzie, C. W. Hicks, N. Kikugawa, S. Raghu, E. D. Bauer, and S. E. Brown, Constraints on the superconducting order parameter in Sr_2RuO_4 from oxygen-17 nuclear magnetic resonance, *Nature (London)* **574**, 72 (2019).
- [17] K. Ishida, M. Manago, K. Kinjo, and Y. Maeno, Reduction of the ^{17}O Knight shift in the superconducting state and the heat-up effect by NMR pulses on Sr_2RuO_4 , *J. Phys. Soc. Jpn.* **89**, 034712 (2020).
- [18] A. N. Petsch, M. Zhu, M. Enderle, Z. Q. Mao, Y. Maeno, I. I. Mazin, and S. M. Hayden, Reduction of the Spin Susceptibility in the Superconducting State of Sr_2RuO_4 Observed by Polarized Neutron Scattering, *Phys. Rev. Lett.* **125**, 217004 (2020).
- [19] H. S. Røising, T. Scaffidi, F. Flicker, G. F. Lange, and S. H. Simon, Superconducting order of Sr_2RuO_4 from a three-dimensional microscopic model, *Phys. Rev. Research* **1**, 033108 (2019).
- [20] A. T. Rømer, D. D. Scherer, I. M. Eremin, P. J. Hirschfeld, and B. M. Andersen, Knight Shift and Leading Superconducting Instability from Spin Fluctuations in Sr_2RuO_4 , *Phys. Rev. Lett.* **123**, 247001 (2019).
- [21] W.-S. Wang, C.-C. Zhang, F.-C. Zhang, and Q.-H. Wang, Theory of Chiral p -Wave Superconductivity with Near Nodes for Sr_2RuO_4 , *Phys. Rev. Lett.* **122**, 027002 (2019).
- [22] Z. Wang, X. Wang, and C. Kallin, Spin-orbit coupling and spin-triplet pairing symmetry in Sr_2RuO_4 , *Phys. Rev. B* **101**, 064507 (2020).
- [23] H. G. Suh, H. Menke, P. M. R. Brydon, C. Timm, A. Ramires, and D. F. Agterberg, Stabilizing even-parity chiral superconductivity in Sr_2RuO_4 , *Phys. Rev. Research* **2**, 032023(R) (2020).
- [24] A. T. Rømer, A. Kreisel, M. A. Müller, P. J. Hirschfeld, I. M. Eremin, and B. M. Andersen, Theory of strain-induced magnetic order and splitting of T_c and T_{TRSB} in Sr_2RuO_4 , *Phys. Rev. B* **102**, 054506 (2020).
- [25] S. A. Kivelson, A. C. Yuan, B. Ramshaw, and R. Thomale, A proposal for reconciling diverse experiments on the superconducting state in Sr_2RuO_4 , *npj Quantum Mater.* **5**, 43 (2020).
- [26] R. Sharma, S. D. Edkins, Z. Wang, A. Kostin, C. Sow, Y. Maeno, A. P. Mackenzie, J. C. S. Davis, and V. Madhavan, Momentum-resolved superconducting energy gaps of Sr_2RuO_4 from quasiparticle interference imaging, *Proc. Natl. Acad. Sci. (USA)* **117**, 5222 (2020).
- [27] G. M. Luke, Y. Fudamoto, K. M. Kojima, M. I. Larkin, J. Merrin, B. Nachumi, Y. J. Uemura, Y. Maeno, Z. Q. Mao, Y. Mori, H. Nakamura, and M. Sigrist, Time-reversal symmetry-breaking superconductivity in Sr_2RuO_4 , *Nature (London)* **394**, 558 (1998).
- [28] V. Grinenko, R. Sarkar, K. Kihou, C. H. Lee, I. Morozov, S. Aswartham, B. Büchner, P. Chekhonin, W. Skrotzki, K. Nenkov, R. Hühne, K. Nielsch, S. L. Drechsler, V. L. Vadimov, M. A. Silaev, P. A. Volkov, I. Eremin, H. Luetkens, and H. H. Klauss, Superconductivity with broken time-reversal symmetry inside a superconducting s-wave state, *Nat. Phys.* **16**, 789 (2020).
- [29] J. Xia, Y. Maeno, P. T. Beyersdorf, M. M. Fejer, and A. Kapitulnik, High Resolution Polar Kerr Effect Measurements of Sr_2RuO_4 : Evidence for Broken Time-Reversal Symmetry in the Superconducting State, *Phys. Rev. Lett.* **97**, 167002 (2006).
- [30] I. Schnell, I. I. Mazin, and A. Y. Liu, Unconventional superconducting pairing symmetry induced by phonons, *Phys. Rev. B* **74**, 184503 (2006).
- [31] M. Braden, A. H. Moudden, S. Nishizaki, Y. Maeno, and T. Fujita, Structural analysis of Sr_2RuO_4 , *Phys. C* **273**, 248 (1997).
- [32] M. Braden, W. Reichardt, Y. Sidis, Z. Mao, and Y. Maeno, Lattice dynamics and electron-phonon coupling in Sr_2RuO_4 : Inelastic neutron scattering and shell-model calculations, *Phys. Rev. B* **76**, 014505 (2007).
- [33] Z. Fang and K. Terakura, Magnetic phase diagram of $\text{Ca}_{2-x}\text{Sr}_x\text{RuO}_4$ governed by structural distortions, *Phys. Rev. B* **64**, 020509(R) (2001).
- [34] O. Friedt, M. Braden, G. André, P. Adelman, S. Nakatsuji, and Y. Maeno, Structural and magnetic aspects of the metal-insulator transition in $\text{Ca}_{2-x}\text{Sr}_x\text{RuO}_4$, *Phys. Rev. B* **63**, 174432 (2001).
- [35] M. Braden, W. Reichardt, S. Shiryayev, and S. Barilo, Giant phonon anomalies in the bond-stretching modes in doped BaBiO_3 : comparison to cuprates manganites and nickelates, *Physica C* **378-381**, 89 (2002).
- [36] Y. Wang, J. J. Wang, J. E. Saal, S. L. Shang, L.-Q. Chen, and Z.-K. Liu, Phonon dispersion in Sr_2RuO_4 studied by a first-principles cumulative force-constant approach, *Phys. Rev. B* **82**, 172503 (2010).
- [37] M. Braden, L. Pintschovius, T. Uefuji, and K. Yamada, Dispersion of the high-energy phonon modes in $\text{Nd}_{1.85}\text{Ce}_{0.15}\text{CuO}_4$, *Phys. Rev. B* **72**, 184517 (2005).
- [38] T. Imai, A. W. Hunt, K. R. Thurber, and F. C. Chou, ^{17}O NMR evidence for orbital dependent ferromagnetic correlations in Sr_2RuO_4 , *Phys. Rev. Lett.* **81**, 3006 (1998).
- [39] Y. Sidis, M. Braden, P. Bourges, B. Hennion, S. Nishizaki, Y. Maeno, and Y. Mori, Evidence for Incommensurate Spin Fluctuations in Sr_2RuO_4 , *Phys. Rev. Lett.* **83**, 3320 (1999).
- [40] M. Braden, Y. Sidis, P. Bourges, P. Pfeuty, J. Kulda, Z. Mao, and Y. Maeno, Inelastic neutron scattering study of magnetic excitations in Sr_2RuO_4 , *Phys. Rev. B* **66**, 064522 (2002).
- [41] F. Servant, B. Fåk, S. Raymond, J. P. Brison, P. Lejay, and J. Flouquet, Magnetic excitations in the normal and superconducting states of Sr_2RuO_4 , *Phys. Rev. B* **65**, 184511 (2002).
- [42] M. Braden, P. Steffens, Y. Sidis, J. Kulda, P. Bourges, S. Hayden, N. Kikugawa, and Y. Maeno, Anisotropy of the Incommensurate Fluctuations in Sr_2RuO_4 : A Study with Polarized Neutrons, *Phys. Rev. Lett.* **92**, 097402 (2004).
- [43] K. Iida, M. Kofu, N. Katayama, J. Lee, R. Kajimoto, Y. Inamura, M. Nakamura, M. Arai, Y. Yoshida, M. Fujita, K. Yamada, and S.-H. Lee, Inelastic neutron scattering study of the magnetic fluctuations in Sr_2RuO_4 , *Phys. Rev. B* **84**, 060402(R) (2011).

- [44] K. Iida, J. Lee, M. B. Stone, M. Kofu, Y. Yoshida, and S. Lee, Two-dimensional incommensurate magnetic fluctuations in $\text{Sr}_2(\text{Ru}_{0.99}\text{Ti}_{0.01})\text{O}_4$, *J. Phys. Soc. Jpn.* **81**, 124710 (2012).
- [45] P. Steffens, Y. Sidis, J. Kulda, Z. Q. Mao, Y. Maeno, I. I. Mazin, and M. Braden, Spin Fluctuations in Sr_2RuO_4 from Polarized Neutron Scattering: Implications for Superconductivity, *Phys. Rev. Lett.* **122**, 047004 (2019).
- [46] M. Braden, O. Friedt, Y. Sidis, P. Bourges, M. Minakata, and Y. Maeno, Incommensurate Magnetic Ordering in $\text{Sr}_2\text{Ru}_{1-x}\text{Ti}_x\text{O}_4$, *Phys. Rev. Lett.* **88**, 197002 (2002).
- [47] J. P. Carlo, T. Goko, I. M. Gat-Malureanu, P. L. Russo, A. T. Savici, A. A. Aczel, G. J. MacDougall, J. A. Rodriguez, T. J. Williams, G. M. Luke, C. R. Wiebe, Y. Yoshida, S. Nakatsuji, Y. Maeno, T. Taniguchi, and Y. J. Uemura, New magnetic phase diagram of $(\text{Sr}, \text{Ca})_2\text{RuO}_4$, *Nat. Mater.* **11**, 323 (2012).
- [48] S. Kunkemöller, A. A. Nugroho, Y. Sidis, and M. Braden, Spin-density-wave ordering in $\text{Ca}_{0.5}\text{Sr}_{1.5}\text{RuO}_4$ studied by neutron scattering, *Phys. Rev. B* **89**, 045119 (2014).
- [49] B. Zinkl and M. Sigrist, Impurity induced double transitions for accidentally degenerate unconventional pairing states, *Phys. Rev. Research* **3**, L012004 (2021).
- [50] I. I. Mazin and D. J. Singh, Competitions in Layered Ruthenates: Ferromagnetism Versus Antiferromagnetism and Triplet Versus Singlet Pairing, *Phys. Rev. Lett.* **82**, 4324 (1999).
- [51] J.-W. Huo, T. M. Rice, and F.-C. Zhang, Spin Density Wave Fluctuations and p -Wave Pairing in Sr_2RuO_4 , *Phys. Rev. Lett.* **110**, 167003 (2013).
- [52] S. Kunkemöller, P. Steffens, P. Link, Y. Sidis, Z. Q. Mao, Y. Maeno, and M. Braden, Absence of a Large Superconductivity-Induced Gap in Magnetic Fluctuations of Sr_2RuO_4 , *Phys. Rev. Lett.* **118**, 147002 (2017).
- [53] K. Iida, M. Kofu, K. Suzuki, N. Murai, S. Ohira-Kawamura, R. Kajimoto, Y. Inamura, M. Ishikado, S. Hasegawa, T. Masuda, Y. Yoshida, K. Kakurai, K. Machida, and S. Lee, Horizontal line nodes in Sr_2RuO_4 proved by spin resonance, *J. Phys. Soc. Jpn.* **89**, 053702 (2020).
- [54] Y. Maeno, K. Yoshida, H. Hashimoto, S. Nishizaki, S.-i. Ikeda, M. Nohara, T. Fujita, A. Mackenzie, N. Hussey, J. Bednorz, and F. Lichtenberg, Two-dimensional Fermi liquid behavior of the superconductor Sr_2RuO_4 , *J. Phys. Soc. Jpn.* **66**, 1405 (1997).
- [55] H. Mukuda, K. Ishida, Y. Kitaoka, K. Asayama, Z. Q. Mao, Y. Mori, and Y. Maeno, ^{17}O NMR probe of spin fluctuations in triplet superconductor Sr_2RuO_4 , *Phys. B* **259-261**, 944 (1999).
- [56] J. E. Ortmann, J. Y. Liu, J. Hu, M. Zhu, J. Peng, M. Matsuda, X. Ke, and Z. Q. Mao, Competition between antiferromagnetism and ferromagnetism in Sr_2RuO_4 probed by Mn and Co doping, *Sci. Rep.* **3**, 2950 (2013).
- [57] H. U. R. Strand, M. Zingl, N. Wentzell, O. Parcollet, and A. Georges, Magnetic response of Sr_2RuO_4 : Quasi-local spin fluctuations due to Hund's coupling, *Phys. Rev. B* **100**, 125120 (2019).
- [58] T. Moriya, *Spin Fluctuations in Itinerant Electron Magnetism* (Springer-Verlag, Berlin, 1985).
- [59] K. Jenni, S. Kunkemöller, D. Brüning, T. Lorenz, Y. Sidis, A. Schneidewind, A. A. Nugroho, A. Rosch, D. I. Khomskii, and M. Braden, Interplay of Electronic and Spin Degrees in Ferromagnetic SrRuO_3 : Anomalous Softening of the Magnon Gap and Stiffness, *Phys. Rev. Lett.* **123**, 017202 (2019).
- [60] C. N. Veenstra, Z. H. Zhu, B. Ludbrook, M. Capsoni, G. Levy, A. Nicolaou, J. A. Rosen, R. Comin, S. Kittaka, Y. Maeno, I. S. Elfimov, and A. Damascelli, Determining the Surface-to-Bulk Progression in the Normal-State Electronic Structure of Sr_2RuO_4 by Angle-Resolved Photoemission and Density Functional Theory, *Phys. Rev. Lett.* **110**, 097004 (2013).
- [61] K. Jenni, M. Braden, Y. Sidis, and P. Steffens, Interplay of magnetic excitations and superconductivity in Sr_2RuO_4 (2018), Institut Laue-Langevin (ILL), doi:10.5291/ILL-DATA.4-02-537.
- [62] K. Jenni, M. Braden, Y. Sidis, and P. Steffens, π,π resonance mode in the superconducting state of Sr_2RuO_4 (2020), Institut Laue-Langevin (ILL), doi:10.5291/ILL-DATA.4-02-586.
- [63] K. Jenni, M. Braden, Y. Sidis, and P. Steffens, Electronic interaction in the unconventional superconductor Sr_2RuO_4 (2020), Institut Laue-Langevin (ILL), doi:10.5291/ILL-DATA.4-02-565.
- [64] M. Braden, K. Jenni, D. Voneshen, Y. Sidis, P. Steffens, and S. Kunkemöller, Low-energy magnetic excitations in the superconducting state of Sr_2RuO_4 : opening of a gap? (2017), STFC ISIS Neutron and Muon Source, doi:10.5286/ISIS.E.RB1710381.
- [65] I. I. Mazin, D. J. Singh, M. D. Johannes, and M. H. Du, Unconventional Superconductivity with a Sign Reversal in the Order Parameter of $\text{LaFeAsO}_{1-x}\text{F}_x$, *Phys. Rev. Lett.* **101**, 057003 (2008).